Master of Science Thesis in
Medical Radiation Physics

MRI-Based Quantification of Intra-Myocellular Fat Content

Pernilla Peterson

Supervisor: Sven Månsson

The work has been performed at:
Department of Medical Radiation Physics,
Malmö University Hospital
AstraZeneca R&D, Mölndal

Medical Radiation Physics
Clinical Sciences, Lund
Lund University, 2009

Abstract

Introduction
Cardiac steatosis, or overstorage of fat in the cardiac muscle cells, is a possible side effect from drugs treating diabetes mellitus. Therefore, a non-invasive means of fat quantification is needed during drug development. The aim of this master thesis is to develop a method to quantify the fraction intra-myocellular fat in the cardiac muscle of rats using magnetic resonance imaging (MRI). Simulations, *in vitro* experiments on phantoms and *in vivo* experiments on rats were conducted during development and the quantification accuracy of the method was compared to that of magnetic resonance spectroscopy (MRS).

Theory
Multi-echo imaging is based on the Dixon technique which is a method for fat/water separation. The method uses the chemical shift between water and fat to separate the species from a number of acquired gradient echoes with different TEs. The reconstruction includes built-in corrections for T_2*-relaxation, off-resonance effects and the multi-resonance signal of fat. To obtain a quantitative measure of the volume fat fraction, corrections for bias from differences in relaxation times and proton density are included.

Material and methods
Initially, simulations were performed in Matlab to learn more about the method and its properties. Intralipid phantoms were created with volume fat fractions ranging from 0 % to 21.7 % and measured with multi-echo imaging and spectroscopy at 1.5 T and 3 T Siemens scanners. The method was also tested *in vivo* by animal experiments on rats fed with a steatosis-inducing drug using a 4.7 T Bruker system.

Results
Simulations showed that the use of a lower magnetic field strength and a fewer number of echoes is less sensitive to inaccuracies in the modelled fat spectrum. *In vitro*, the method successfully quantified fat fractions as low as 0.2 % with quantification accuracy similar to that of spectroscopy. *In vivo*, however, no correlation could be detected between spectroscopy and imaging results.

Conclusion
Although the method is still to be successfully tested *in vivo*, it does show potential to be applicable also in living tissue. This potential may be greater in organs were the fat content is higher and the movements less problematic than in the heart.

Table of contents

Abbreviations and symbols

Abbreviations

DESPOT	Driven-equilibrium single-pulse observation of T_1
ECG	Electrocardiography
EMCL	Extra-myocellular lipids
FF	Fat fraction
FID	Free induction decay
FOV	Field of view
IMCL	Intra-myocellular lipids
MGE	Multi gradient echo
MRI	Magnetic resonance imaging
MRS	Magnetic resonance spectroscopy
NEX	Number of signal excitations
NSA	Effective number of signal averages
TI	Time from inversion
PRESS	Point resolved spectroscopy
RF	Radio frequency
ROI	Region of interest
SNR	Signal to noise ratio
TE	Echo time
TR	Repetition time

Symbols

t	Echo time
$s(t)$	Total signal at the echo time t
W	Water volume
F	Fat volume
$\tilde{\tilde{w}}$	Estimated water volume
$\tilde{\tilde{f}}$	Estimated fat volume
η	Signal contributions from water (indexed w) or fat (indexed f)
$\tilde{\tilde{\eta}}$	Estimated signal contribution from water (indexed w) or fat (indexed f)
α_m	Amplitude of fat peak m
$\Delta f_{f,m}$	Resonance frequency of fat peak m
M	Number of fat resonances
ψ	Magnetic field offset
$\hat{\psi}$	Complex field map
$\tilde{\tilde{\psi}}$	Estimated complex field map
n	Noise
N	Number of acquired echoes
θ	Flip angle
σ_s	Variance of the noise in the acquired images
σ_ρ	Variance of the noise in the estimated water and fat signals
M_0	Magnetization immediately after the excitation pulse
S	Signal from the indexed pulse sequence
ρ	Proton density of fat (indexed w) or fat (indexed f)

1.Introduction

The aim of this master thesis is to develop a method to quantify the fraction intra-myocellular fat in the cardiac muscle of rats using magnetic resonance imaging (MRI). The quantitative measure used is the volume fat fraction (FF), defined as:

$$FF = \frac{F}{W + F} \qquad \text{(Eq.1)}$$

where F is the fat volume content and W is the water volume content.

The developed imaging method is tested *in vitro* through a phantom study and *in vivo* through animal experiments on rats and the quantification accuracy is compared to that of magnetic resonance spectroscopy (MRS). Also, simulations are used during development and optimization of the method. The results from the *in vitro* study has been submitted to and accepted for oral presentation at the 26th annual European Society for Magnetic Resonance in Medicine and Biology meeting.

This study was part of an AstraZeneca R&D project which aimed at investigating the possibilities of using MRI to determine increased intra-myocellular fat content and its influence on the heart function in rats. The results are compared with histopathological findings. If feasible, the imaging method is valuable to evaluate the extent of cardiac steatosis (see below) as a safety biomarker in the development of drugs treating diabetes mellitus. This thesis focuses on the development of a non-invasive method of fat quantification and does not include methodology and results from the investigation of cardiac function.

1.1. Background

1.1.1. Fat

Fat, or triacylglycerol, consists of a glycerol molecule in which the three –OH-groups have been replaced by fatty acids. Fatty acids are aliphatic chains consisting of between four and 22 carbon atoms [1]. The various protons have resonance frequencies that depend on their place in the fatty acid chain. The contributions to the fat signal (spectrum from the nutritional supplement Intralipid) are summarized in Table 1 below.

Fat is stored in the body as subcutaneous or interstitial adipose tissue, i.e. in adipocytes which are cells specialized in storing energy as fat. The fat in adipocytes is stored as a large fat droplet covering the majority of the cell volume; this fat is referred to as extra-myocellular lipids (EMCL). Intra-myocellular lipids (IMCL), which are the lipids of interest in cardiac steatosis, are stored in muscle cells (myocytes) as small droplets in close proximity to the mitochondria [2,3]. The chemical shift of EMCL and IMCL differs by approximately 0.2 ppm.

Table 1. Contributions to the MRS fat signal in Intralipid where the protons in bold give rise to the respective frequencies. The spectrum is collected from Intralipid using a 4.7 T Bruker system (Figure 1) [own data]. Peak no 10 was not detectable in the spectrum.

Peak number	*Relative amplitude (%)*	*Shift relative water (ppm)*	*Proton*	*Group*	*Compound*
1	61.5	-3.55	- $(C\mathbf{H_2})_n$ -	Methylene	All fatty acid chains

Peak number	*Relative amplitude (%)*	*Shift relative water (ppm)*	*Proton*	*Group*	*Compound*
2	9.8	-3.96	- CH_2 - CH_2 - CH_2 - $C\mathbf{H_3}$	Methyl	All fatty acid chains except linolenic
3	8.0	0.47	- C**H** = C**H** -	Olefin	All unsaturated fatty acids
4	7.7	-2.81	- $C\mathbf{H_2}$ - CH = CH -	α-olefin	All unsaturated fatty acids
5	4.2	-2.61	- CH_2 - $C\mathbf{H_2}$ - COOR	α-carboxyl	All fatty acid chains
6	3.9	-2.09	- CH = CH – $C\mathbf{H_2}$ –CH = CH-	Diacyl	Linoleic and linolenic acid
7	2.1	-3.25	- $C\mathbf{H_2}$ - CH_2 - COOR	β-carboxyl	All fatty acid chains
8	1.5	-0.58	- CH – $C\mathbf{H_2}$ – O-CO-R_1	Glycerol	All triacylglycerides
9	1.4	-0.76	- CH – $C\mathbf{H_2}$ – O-CO-R_3	Glycerol	All triacylglycerides
10	-	-	- CH_2 – C**H** – CH_2 -	Glycerol	All triacylglycerides

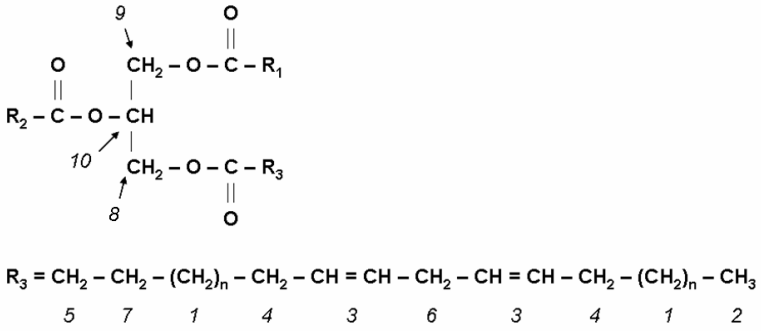

Figure 1. Example of a triacylglyceride molecule. The top molecule is a glycerol molecule with the fatty acid chains R_1, R_2, and R_3 attached. R_3 is shown as an example. The numbers in italic indicate the numbers that represent the group throughout this report. Figure adapted from Szczepaniak *et al.* [4].

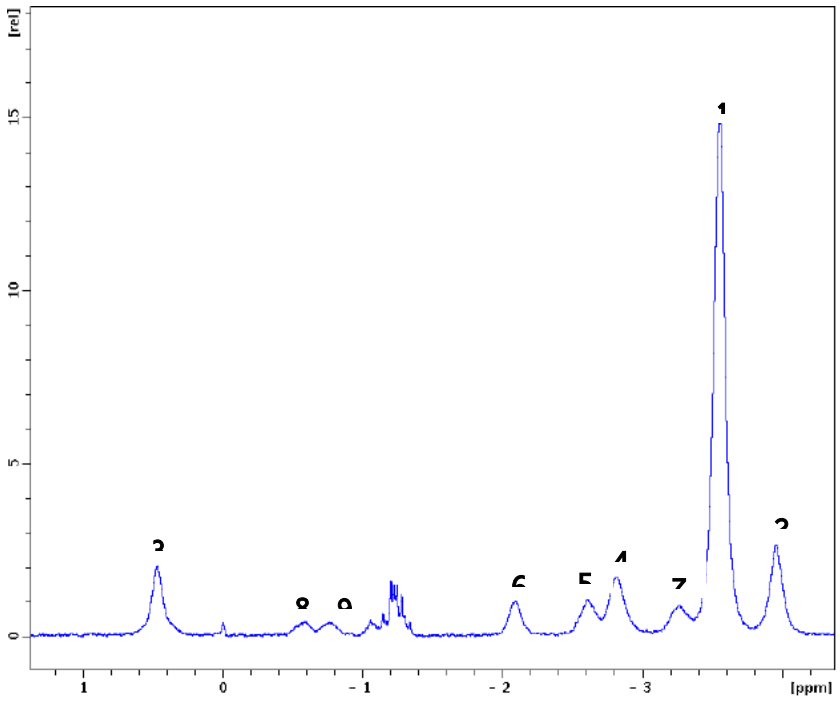

Figure 2. Spectrum acquired from Intralipid at a 4.7 T Bruker scanner. The numbers refer to the signal origin and are explained in Table 1 and Figure 1.

1.1.2. Cardiac steatosis

Free fatty acids are used by the cardiomyocytes, as by other muscle cells, to generate adenosine triphosphate (ATP). The excess is stored as a reserve in the form of triacylglycerides. An increased level of free fatty acids in the blood plasma, e.g. caused by a disturbed glucose uptake in patients with diabetes mellitus, can increase the stored levels of triacylglycerides in the myocardium [5]. This overstorage of fat is called cardiac steatosis and

is expected to cause volume fat fractions of approximately 1.1 % compared to 0.5 % in a healthy cardiac muscle [6]. The possible consequences of steatosis on cardiac function remain unclear [5].

1.1.3. Methods for quantification of IMCL

A number of methods for quantification of IMCL exist and quite a few of them are related to this project. The histopathological group of methods includes Oil Red O staining during which fat is visualized in red under a light microscope. Using a digital image, the volume of the cell consisting of fat can be determined. However, only small tissue samples can be analyzed and there is a risk of staining also metabolites of fatty acids [3].

The non-invasive methods include MRS and MRI. The obvious advantage of the latter is the resulting image in which a heterogeneous distribution of accumulated fat can be detected. In localized MRS the placement of the voxel is critical and the risk of contamination from surrounding tissues is high. Voxel placement is further complicated by the chemical shift between fat and water which causes two separate voxel positions of the species. An advantage of MRS is that a high enough resolution of the spectrum makes the distinction between EMCL and IMCL possible in contrast to when using MRI [3].

A method not used in this work that yields both spectral and spatial information is magnetic resonance spectroscopic imaging (MRSI). Through the use of phase encoding gradients, as used in MRI, an array of spectroscopic voxels can be obtained and registered to a structural MR-image. The major disadvantage of this method is the spatial encoding technique which gives rise to lengthy data collections even for low resolutions. Often, as few as 8x8 voxels are practically possible *in vivo* [7].

2. Theory

2.1. The Dixon method

The two-point Dixon method was originally proposed as a means of separating water and fat signals using the chemical shift between them (approximately -3.5 ppm) [8]. The difference in resonance frequencies causes the magnetization vectors of water and fat to be in- or out-of-phase at different time points after the excitation pulse. The in-phase signal is the sum of the fat and water signal contributions whereas the out-of-phase signal is the difference (Figure 3). By acquiring two images, one at each of these time points, the water and fat components of the signal can be estimated through an analytical solution of a linear equation system.

This is possible both using magnitude and complex data. The magnitude data consists only of the signal vector length whereas the complex data contains information also about the phase angle.

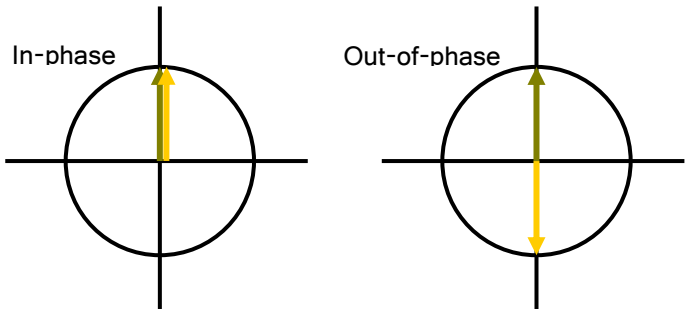

Figure 3. The basic idea behind the two-point Dixon method. The in-phase signal is the sum of the water (green) and fat (yellow) signal contributions and the out-of-phase signal is the difference.

2.2. Multi-echo imaging

Of course, the signal is also affected by other factors such as field inhomogeneities, T_1-, T_2- and T_2*-relaxation and the multiple fat resonances. Each of these factors will be further discussed below. In order to solve and correct for these effects, additional echoes need to be acquired and the Dixon-method extended.

In summary, the signal, *s*, from a voxel containing water and fat is given by:

$$s(t) = \left(\eta_w + \eta_f \sum_{m=1}^{M} \alpha_m e^{i2\pi\Delta f_{f,m} t} \right) \cdot e^{i2\pi\psi t} \cdot e^{-R_2' t} + n \qquad \text{(Eq.2)}$$

The water and fat signal contributions are given by η_w and η_f, respectively. The echo time, *t*, is defined as the time between the excitation pulse and the data collection in a gradient echo sequence (see Section 2.4). α_m is the relative amplitude of the fat component *m* with the frequency shift $\Delta f_{F,m}$, ψ is the local magnetic resonance offset, $R_2' = 1/T_2'$ (see Eq.5, Section 2.2.2) and *n* is the noise. The frequency of fat is defined relative to the water frequency.

In case of multi-echo imaging, using *N* echoes, it is easier to deal with the signal expression in matrix form:

$$S = D \cdot A \cdot \eta \qquad \text{(Eq.3)}$$

$$D_{N\times N} = \begin{bmatrix} e^{i2\pi\psi t_1}\cdot e^{-R_2' t_1} & 0 & \dots & 0 \\ 0 & e^{i2\pi\psi t_2}\cdot e^{-R_2' t_2} & \dots & 0 \\ \dots & \dots & \dots & \dots \\ 0 & 0 & \dots & e^{i2\pi\psi t_N}\cdot e^{-R_2' t_N} \end{bmatrix},$$

$$A_{N\times 2} = \begin{bmatrix} 1 & \sum_{m=1}^{M}\alpha_m e^{i2\pi\Delta f_{f,m} t_1} \\ 1 & \sum_{m=1}^{M}\alpha_m e^{i2\pi\Delta f_{f,m} t_2} \\ \dots & \dots \\ 1 & \sum_{m=1}^{M}\alpha_m e^{i2\pi\Delta f_{f,m} t_N} \end{bmatrix}, \quad S_{N\times 1} = \begin{bmatrix} s(t_1) \\ s(t_2) \\ \dots \\ s(t_N) \end{bmatrix}, \quad \eta_{2\times 1} = \begin{bmatrix} \eta_w \\ \eta_f \end{bmatrix}$$

If the magnetic resonance offset, ψ, and T_2' are known, the water and fat signal contributions can be estimated through linear least-squares fitting according to Eq.4, where H indicates the hermitian conjugate [9].

$$\tilde{\eta} = \left(A^H A\right)^{-1} A^H D^{-1} S \qquad \text{(Eq.4)}$$

The phase angle difference of methylene between echo acquisitions is referred to as the echo shift. For example, collecting in- and out-of-phase signals corresponds to an echo shift of 180°. This echo shift is necessary when using magnitude data as the signal vector length otherwise will be affected also by the phase angle.

2.2.1. Fat-fat interactions

As the fat signal arises from a number of protons with different chemical shifts (see Table 2), the phase angle difference between water and the sum of these resonances will differ from the expected in- and out-of-phase positions. The multiple resonances of fat can be taken into account by modelling each of the *M* fat peaks frequencies, $\Delta f_{f,m}$, and amplitudes, α_m, in the signal expression used in the estimation of the fat and water signal contributions:

$$s(t) = \eta_w + \eta_f \sum_{m=1}^{M}\alpha_m e^{i2\pi\Delta f_{f,m} t}$$

Yu *et al.* described two approaches to obtain the peak amplitudes: Pre and self calibration [10]. Both of these methods require *a priori* knowledge of the fat peak positions, which can be determined by spectroscopy, but the former also uses modelled amplitudes. When using the self calibrated method, the amplitudes are estimated in the reconstruction by treating three of the fat peaks as separate species. From selected pixels with a high fat content, average relative amplitudes are calculated in the estimated fat images. These estimated relative amplitudes are then used in the reconstruction of a fat fraction image. As this approach requires fat rich pixels, it is not applicable in the case when the expected fat fractions are small [10].

The amplitudes of the fat peaks depend on the type of fatty acids that are attached to the triacylglyceride molecules. The frequency shift between water and fat depends on two factors: the temperature and bulk susceptibility effects [2,4,11]. The temperature dependence on the chemical shift is caused by the electron configurations effect on the magnetic field felt by the hydrogen proton in a water molecule. When raising the temperature, the nature of the hydrogen bonds between water molecules alters, leading to an increased electron screening efficiency of the proton. This leads to an altered water resonance frequency. The resonance frequencies of fat will not be as affected by the change in temperature and thus the shift between water and fat resonances is temperature dependent. A temperature difference of 10 °C causes a frequency shift of approximately 0.1 ppm [11].

The magnetic field depends locally on susceptibility variations which depend on the way fat is structured in the surrounding medium. The susceptibility variations cause a shift of the position of the entire fat spectrum relative to the water peak position [2,4]. Correctly modelled fat peak positions should thus be based on a medium in which fat is structured in a similar fashion as IMCL. The nutritional supplement Intralipid consists of soybean oil droplets dispersed in water (0.2 g/ml soybean oil, 12 g/ml lecithin, 22 g/ml glycerol and sodium hydroxide), much like the droplets of IMCL in the cell cytoplasm. For this reason, Intralipid is used as a model for fat frequencies and amplitudes throughout this work (see Table 2). The volume fat fraction of Intralipid (excluding lecithin and glycerol) is 21.7 %.

Table 2. Fat peak positions in Intralipid measured at a 4.7 T Bruker scanner [own data].

Peak nr	*Relative amplitude (%)*	*Chemical shift (ppm)*
1	61.5	-3.55
2	9.8	-3.96
3	8.0	0.47
4	7.7	-2.81
5	4.2	-2.61
6	3.9	-2.09
7	2.1	-3.25
8	1.5	-0.58
9	1.4	-0.76

2.2.2. Off-resonance effects and T_2'-relaxation

Both the phase angle of the signal and the signal strength are affected by local variations of the field strength. These field inhomogeneities cause altered resonance frequencies, an off-resonance effect, and the decay of the longitudinal magnetization over time through T_2*-relaxation. T_2*-relaxation is made up by the T_2-relaxation and a term proportional to the inhomogeneity. This decay limits the number of echoes that can be acquired [12].

$$\frac{1}{T_2 *} = \frac{1}{T_2} + \frac{1}{T_2'} \qquad \text{(Eq.5)}$$

$$\frac{1}{T_2'} \sim \gamma \Delta B_0$$

The off-resonance effect shifts the expected phases of water and fat, but the phase difference between them is unaffected because their respective resonance frequencies are equally

affected (Figure 4). Hence, the magnitude of the total signal is insensitive to off-resonance and thus the use of magnitude data requires no correction for the off-resonance effect. However, this correction is necessary when using complex data.

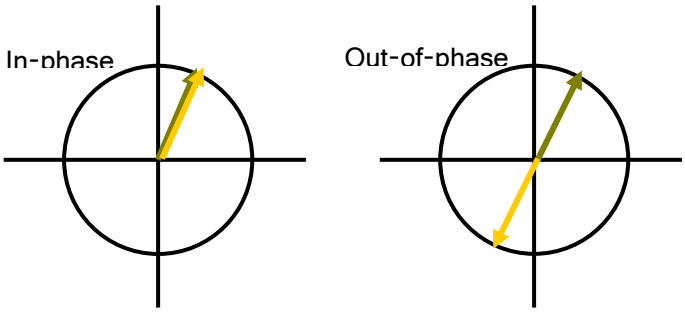

Figure 4. The field inhomogeneity problem. The water (green) and fat (yellow) magnetization vectors are equally affected by the inhomogeneities and thus the shift between them are unaffected.

In case of off-resonance, the phase angle of the magnetization vector of water linearly increases with time where the slope determines the size of the off-resonance effect. When the fat fraction is very low, the phase contribution from the magnetization vector of fat can be neglected. In this case, the effect can be corrected for by the use of the slope of the signal phase angle over time, possibly after unwrapping to avoid discontinuities. Large enough off-resonances can cause phase errors that are larger than 360°. These cannot be distinguished from the corresponding smaller phase errors and this causes leaps in the phase angle over time data. Unwrapping is the procedure that locates these discontinuities and corrects them. This correction will be referred to as the off-resonance correction. In the case of higher fat fractions, an iterative calculation of the field map is necessary [8,13].

Both of the effects caused by a inhomogeneous field can be combined into a complex field map, $\hat{\psi}$. The signal expression, excluding noise for convenience, becomes [14]:

$$s(t) = \left(\eta_w + \eta_f \sum_{m=1}^{M} \alpha_m e^{i2\pi\Delta f_{f,m} t}\right) \cdot e^{i2\pi\psi t} \cdot e^{-R_2' t} = \left(\eta_w + \eta_f \sum_{m=1}^{M} \alpha_m e^{i2\pi\Delta f_{f,m} t}\right) \cdot e^{i2\pi\left(\psi + \frac{iR_2'}{2\pi}\right)t}$$

$$= \left(\eta_w + \eta_f \sum_{m=1}^{M} \alpha_m e^{i2\pi\Delta f_{f,m} t}\right) \cdot e^{i2\pi\hat{\psi} t}$$

$$\hat{\psi} = \psi + \frac{iR_2'}{2\pi} \qquad \text{(Eq.6)}$$

By using the complex field map, the size of the off-resonance and T_2'-relaxation can be estimated as a single estimator in a single iterative procedure. The practical implementation of the iteration used in this work, which is described further below, is a slightly adjusted version of the technique presented by Yu *et al.* where the complex field map estimated in each step is used as a starting point in the next iteration [14]. In the approach used here, the matrix *A* is corrected after each step in the iteration and the small contributions to the complex field map from each of the steps are added to give the final result. By starting with zero as a first guess of the complex field map, an estimation of the water and fat signals is made with a least squares estimation (**step 1**):

$$\tilde{\eta} = \begin{bmatrix} \tilde{\eta}_w \\ \tilde{\eta}_f \end{bmatrix} = \left(A^H A\right)^{-1} A^H S \qquad \text{(Eq.7)}$$

Using the estimated values in Eq.2 and a Taylor expansion of the term containing the complex field map, the signal can be approximated by:

$$S = \left(\tilde{\eta}_w + \tilde{\eta}_f \sum_{m=1}^{M} \alpha_m e^{i2\pi\Delta f_{f,m} t} \right) e^{i2\pi\tilde{\psi}t} \approx \left(\tilde{\eta}_w + \tilde{\eta}_f \sum_{m=1}^{M} \alpha_m e^{i2\pi\Delta f_{f,m} t} \right) \cdot \left(1 + i2\pi\tilde{\psi}t\right) =$$

$$= i2\pi\tilde{\psi}t \cdot \left(\tilde{\eta}_w + \tilde{\eta}_f \sum_{m=1}^{M} \alpha_m e^{i2\pi\Delta f_{f,m} t} \right) + \left(\tilde{\eta}_w + \tilde{\eta}_f \sum_{m=1}^{M} \alpha_m e^{i2\pi\Delta f_{f,m} t} \right) = B \cdot \begin{bmatrix} \tilde{\psi} \\ \tilde{\eta}_w \\ \tilde{\eta}_f \end{bmatrix} \qquad \text{(Eq.8)}$$

where

$$B = \begin{bmatrix} i2\pi t_1 \left(\tilde{\eta}_w + \tilde{\eta}_f \sum_{m=1}^{M} \alpha_m e^{i2\pi\Delta f_{f,m} t_1} \right) & 1 & \sum_{m=1}^{M} \alpha_m e^{i2\pi\Delta f_{f,m} t_1} \\ i2\pi t_2 \left(\tilde{\eta}_w + \tilde{\eta}_f \sum_{m=1}^{M} \alpha_m e^{i2\pi\Delta f_{f,m} t_2} \right) & 1 & \sum_{m=1}^{M} \alpha_m e^{i2\pi\Delta f_{f,m} t_2} \\ \cdots & \cdots & \cdots \\ i2\pi t_N \left(\tilde{\eta}_w + \tilde{\eta}_f \sum_{m=1}^{M} \alpha_m e^{i2\pi\Delta f_{f,m} t_N} \right) & 1 & \sum_{m=1}^{M} \alpha_m e^{i2\pi\Delta f_{f,m} t_N} \end{bmatrix}$$

The estimated complex field map, $\tilde{\psi}$, can be solved for by using the matrix *B* and the signals S in another least squares estimation (**step 2**) and is used to correct the matrix *A* by a factor $e^{i2\pi\tilde{\psi}t}$ (**step 3**). The two last columns of matrix *B* are identical to the matrix *A* and will thus be altered. The new corrected matrices *A* and *B* are used in a repetition of the procedure from step 1. The complex field map is thus solved in small steps and the contributions are added to give the final result.

Using magnitude data, the complex field map is unnecessary. Instead a similar approach with a modified matrix *B* is used to iteratively solve for the T_2*-relaxation.

$$B = \begin{bmatrix} -t_1 \left(\tilde{\eta}_w + \tilde{\eta}_f \sum_{m=1}^{M} \alpha_m e^{i2\pi\Delta f_{f,m} t_1} \right) & 1 & \sum_{m=1}^{M} \alpha_m e^{i2\pi\Delta f_{f,m} t_1} \\ -t_2 \left(\tilde{\eta}_w + \tilde{\eta}_f \sum_{m=1}^{M} \alpha_m e^{i2\pi\Delta f_{f,m} t_2} \right) & 1 & \sum_{m=1}^{M} \alpha_m e^{i2\pi\Delta f_{f,m} t_2} \\ \cdots & \cdots & \cdots \\ -t_N \left(\tilde{\eta}_w + \tilde{\eta}_f \sum_{m=1}^{M} \alpha_m e^{i2\pi\Delta f_{f,m} t_N} \right) & 1 & \sum_{m=1}^{M} \alpha_m e^{i2\pi\Delta f_{f,m} t_N} \end{bmatrix}$$

2.2.3. Differences in relaxation times and proton densities

Based on the separated water and fat signal images, a signal fat fraction can be calculated. However, the aim of this work is to obtain the volume fat fraction. In order to convert the signal fraction to the volume fraction, the differences in relaxation times and proton density, ρ, between fat and water have to be accounted for, as they will bias the estimated volume fat fraction; e.g. the shorter T_1 of fat can cause an apparently larger fat signal depending on the T_1-weighting of the measurement.

In a spoiled gradient echo sequence the steady-state signal from water (for example), S_{GRE}, is [12]:

$$S_{GRE,w} = \frac{M_{0,w} \cdot \rho_w \cdot \sin(\theta) \cdot \left(1 - e^{-\frac{TR}{T_{1,w}}}\right)}{1 - \cos(\theta) \cdot e^{-\frac{TR}{T_{1,w}}}} \cdot e^{-\frac{TE}{T_{2,w}^*}} = \eta_w \qquad \text{(Eq.9)}$$

The size of the magnetization vectors of water and fat, $M_{0,w}$ and $M_{0,f}$, immediately after the excitation pulse will be dependent on the water or fat volumes and can be used to calculate the volume fat fraction (Eq.1).

The proton density, ρ, is the number of protons giving signal per volume. The proton density of fat can be theoretically calculated to 96 % of that of water by using the densities, molecular weights and molecular formulas of soybean oil and water [15]. Knowing this, Eq.9 can be used to correct the estimated water and fat signal contributions for the proton density differences.

In vivo, the large impact of T_2' will outweigh the effect of the differences in T_2 making them negligible. T_2* of fat and water are thus approximately equal as T_2' is only dependent on the variations in field strength (see Eq.5). *In vitro*, this assumption is not valid because of the higher achievable field homogeneity that will enhance the effect of T_2 in comparison to the lower T_2'. In this case, T_2-values for water and fat from literature or measurements can be incorporated in the matrix A to achieve T_2-corrected signal contributions of fat and water according to:

$$A_{N\times 2} = \begin{bmatrix} e^{-\frac{t_1}{T_{2,w}}} & e^{-\frac{t_1}{T_{2,f}}} \cdot \sum_{m=1}^{M} \alpha_m e^{i2\pi\Delta f_{f,m} t_1} \\ e^{-\frac{t_2}{T_{2,w}}} & e^{-\frac{t_2}{T_{2,f}}} \cdot \sum_{m=1}^{M} \alpha_m e^{i2\pi\Delta f_{f,m} t_2} \\ \cdots & \cdots \\ e^{-\frac{t_N}{T_{2,w}}} & e^{-\frac{t_N}{T_{2,f}}} \cdot \sum_{m=1}^{M} \alpha_m e^{i2\pi\Delta f_{f,m} t_N} \end{bmatrix}$$

The T_1-bias can be avoided by using a small flip angle [16]. This method will be referred to as the small flip angle method. However, the difference in T_1-relaxation time between fat and water can be used to enhance the fat signal and improve the noise performance. If T_1 is known, a simple correction of the biased fat and water signals can be made using Eq.9. This will be referred to as the T_1-corrected method. If this is not the case, or if the effective flip

angle is uncertain, the so called DESPOT (Driven-equilibrium single-pulse observation of T_1) method can be combined with the Dixon method to obtain T_1-maps for fat and water [16]. By collecting data at two flip angles, the T_1-value of water and fat in the separated images can be analytically solved for according to Eq.10 and used to correct for the T_1-bias according to Eq.11. This method will be referred to as the dual flip angle method. In Eq.10 and Eq.11, the case of the T_1-correction of water is presented as an example. The indexed numbers represent the first and second acquired flip angle.

$$e^{-\frac{TR}{T_{1,w}}} = \frac{\tilde{\eta}_{w,1}\cdot\sin(\theta_2) - \tilde{\eta}_{w,2}\cdot\sin(\theta_1)}{\tilde{\eta}_{w,1}\cdot\sin(\theta_2)\cdot\cos(\theta_1) - \tilde{\eta}_{w,2}\cdot\sin(\theta_1)\cdot\cos(\theta_2)} \qquad \text{(Eq.10)}$$

$$\tilde{w} = \frac{\tilde{\eta}_{w,1}\cdot\left(1 - e^{-\frac{TR}{T_{1,w}}}\cos(\theta_1)\right)}{\left(1 - e^{-\frac{TR}{T_{1,w}}}\right)\cdot\sin(\theta_1)} \qquad \text{(Eq.11)}$$

2.3. Noise performance

2.3.1. NSA

When using magnitude data, an accurate estimation of the fat fraction is only possible using an echo shift of 180°, but when using a complex reconstruction any echo shifts are useful. In order to compare magnitude and complex reconstructions, in- and out-of-phase signals should be used. However, the different shifts are more or less advantageous from a noise performance point of view. The effective number of signal averages (NSA) can be used to evaluate the noise performance using different echo shifts. NSA is defined as the mean variance of the noise in the collected images, σ_s, divided by the variance of the estimated water and fat signal contributions, σ_ρ [17].

$$NSA \equiv \frac{\sigma_s}{\sigma_\rho} \qquad \text{(Eq.12)}$$

The highest achievable NSA is equal to the number of acquired echoes and is obtained when the estimated fat or water signals are simple averages of the collected images [17]. In Figure 5, simulated NSA values are shown.[1] The difference between NSA of water and fat is due to fat-fat interactions and the decrease in NSA with increasing echo shift is caused by T_2*-relaxation. According to this simulation, a choice of an echo shift of 180° is still acceptable from a noise performance point of view.

[1] 5000 pixels containing 1 % rapeseed oil was simulated. Eight echoes were acquired using Eq.2 with T_2* = 40 ms, field inhomogeneities of 0.05 ppm and noise corresponding to a SNR of 100 (Eq.13). After a complex reconstruction of the simulated data the variances of the signals and estimated parameters as well as their respective NSA values were calculated according to Eq.12. This was repeated for 100 different echo shifts ranging from zero to 180°.

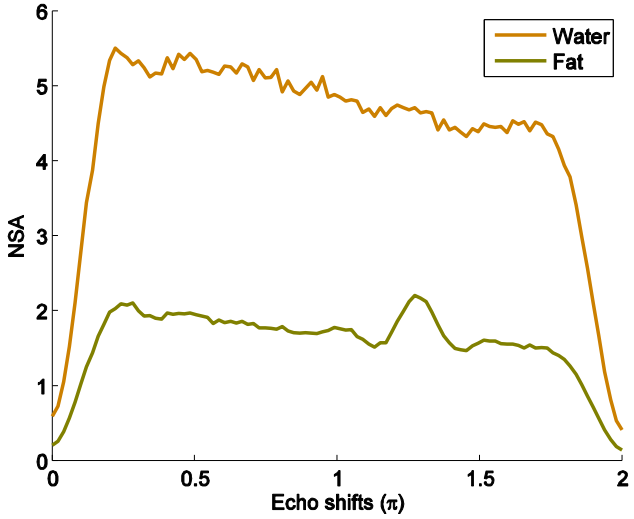

Figure 5. Simulated NSA values for estimated water (brown) and fat (green) contents.

2.3.2. SNR

A more familiar way to quantify the noise performance is the signal to noise ratio, SNR. In this work, SNR is defined as the ratio between the average magnitude signal, $|S|$, in a region of interest (ROI) placed in a signal region and the true standard deviation, σ, within a ROI placed in the background.

$$SNR = \frac{|S|}{\sigma} \qquad \text{(Eq.13)}$$

The true standard deviation of the noise is the standard deviation of each of the real and imaginary components in the complex noise [18]. This value can be estimated from the mean background signal, $\overline{M}$, in the magnitude image:

$$\sigma = \frac{\overline{M}}{\sqrt{\pi/2}}$$

2.4. Pulse sequences

2.4.1. Multi gradient echo

In a multi gradient echo sequence (MGE) a number of gradient echoes are recalled after the excitation pulse and several images with various echo times are obtained. MGE sequences make two collection strategies possible (Figure 6). When using a monopolar approach, data is acquired only when the readout gradient is positive. By acquiring echoes also during the rephasing gradient (bipolar collection) the echo times can be reduced and more echoes collected in the time limit set by the T_2*-decay.

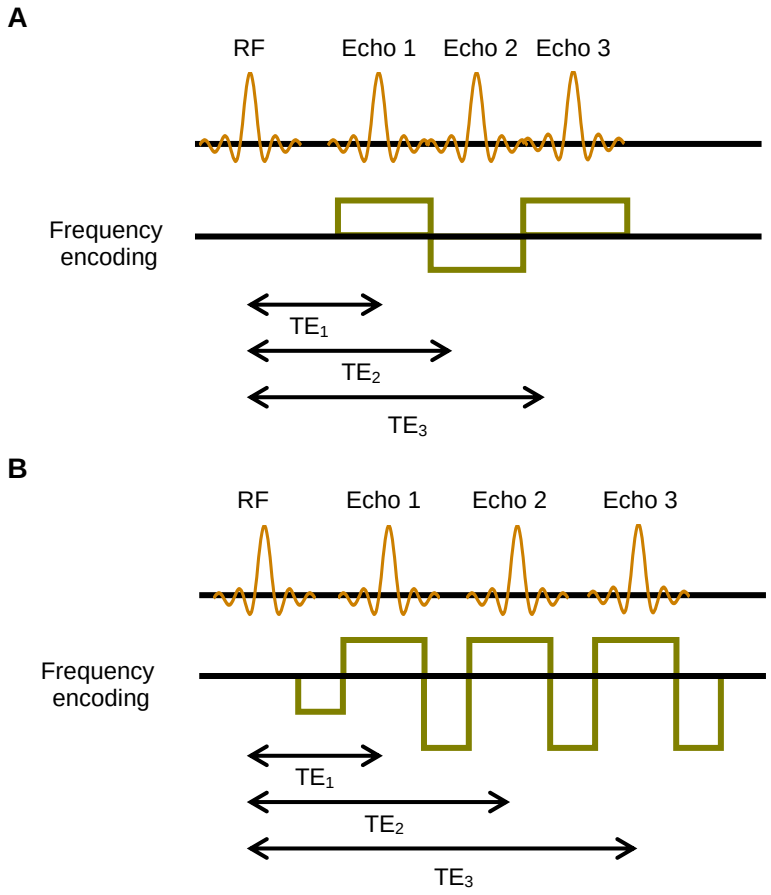

Figure 6. A bipolar (A) and a monopolar (B) approach to data acquisition in an MGE sequence. Using the monopolar approach, data collection has to wait during the rephasing gradient, a delay that is avoided when using the bipolar approach.

2.4.2. PRESS

Point resolved spectroscopy (PRESS) uses a 90° pulse and two 180° pulses applied orthogonally to obtain signal from only a voxel. The free induction decay (FID) is acquired and Fourier transformed in order to obtain a spectrum [19]. The signal expression for a PRESS sequence is given by:

$$S_{PRESS} = M_0\left(1 - e^{-\frac{TR}{T_1}}\right)\cdot e^{-\frac{TE}{T_2}} \qquad \text{(Eq.14)}$$

3. Material and method

During this work, simulations as well as phantom and animal experiments were performed. The simulations were used during optimization of measurement parameters, to estimate limits for the detectable fat fraction and to optimize the techniques used in the method. The developed method was then tested both *in vitro* at clinical 1.5 T and 3 T Siemens scanners and *in vivo* at 4.7 T animal Bruker scanner. Both *in vitro* and *in vivo*, the quantification accuracy was compared to that of MRS.

3.1. Simulations

All simulations were performed in *Matlab* (version R2008a). The effects on the quantification precision by the choice of repetition time and flip angle was examined by simulating three sets of 7000 pixels with the fat fractions 1 %, 5 % and 20 % respectively. Eight echoes were acquired using Eq.2 and Eq.9 with white noise added. TR ranged from 1 ms to 300 ms, the flip angle was varied between 0° and 90°. T_1 was chosen to be 1285 ms for water and 550 ms for fat and the proton density of fat was set to be 96 % of that of water. The pixels were reconstructed and SNR calculated as the mean estimated fat fraction divided by the standard deviation of the estimated fat fraction values. In order to take the maximum practically possible scan time in to account, the reconstruction of the pixels was repeated a number of times that were inversely proportional to TR. For each repetition time, the flip angle corresponding to the maximum SNR was chosen and compared to the Ernst angles of fat and water. This was done for both the signal and the volume fat fractions, that is, both the T_1 and ρ non-corrected and corrected values.

The sensitivity to noise was investigated by simulating data mimicking the animal experiments in regard to SNR, echo shift and ROI size. SNR was approximated to 70, the echo shift chosen to 540° (3x180°) and the ROI size to 100 pixels. T_1 was set to 1285 ms for water and 550 ms for fat; the repetition time was chosen to 500 ms. In order to study the effect on the noise performance by the use of either a small flip angle or a T_1-corrected approach, both the flip angles 8° and 50° was tested.

The standard deviation of the estimated fat fractions was calculated and from them the least detectable fat fraction was estimated.

To simulate the effect of uncertainties and errors in the method and the modelled fat spectrum, simulated noiseless Intralipid data sets were constructed with known volume fat fractions between 0 % and 20 %. Data for eight echoes was generated using Eq.2 with echo times corresponding to in- and out-of-phase signals for the methylene peak of Intralipid and 99 % of this echo shift. T_2* was set to 40 ms and the off-resonance to 0.05 ppm.

In the reconstruction, various numbers of echoes were used (3, 5 or 8) with a shift of the entire fat spectrum of 0.1 ppm compared to the simulated. Field strengths of 1.5 T and 3 T were simulated by changing the resonance frequencies of water and fat and by altering the echo shift. In reality, the echo shift of 540° instead of 180° had to be used due to the larger chemical shift which causes smaller time spacing between the in- and out-of-phase time points at 3 T.

3.2. Phantom measurements

Nine Intralipid (200 mg/ml, Fresnius Kabi) phantoms were prepared in plastic 50 ml vials and diluted with purified water to the fat fractions by volume and proton density given in Table 3. 0.075 mM gadolinium contrast agent (Magnevist, Schering) was added to reduce the T_1 of water to more closely resemble that of muscle tissue. To improve the shimming, the vials were placed standing up in a water filled beaker. The beaker was placed in a birdcage head coil in 1.5 T and 3 T Siemens scanners.

Table 3. Fat fractions by volume and by proton density in Intralipid.

Part Intralipid / part water	*Fat fraction by volume (%)*
1/0	21.7
1/1	10.9
1/3	5.43
1/7	2.72
1/15	1.36
1/31	0.679
1/63	0.340
1/123	0.170
0/1	0

PRESS-localized spectroscopy (Table 4) was performed in each of the nine phantoms and the acquired spectra were analyzed as described in section 3.4.2. T_1-bias of the spectroscopy data was avoided by the use of a long repetition time.

The obtained chemical shift from spectroscopy was used to calculate echo times yielding in- and out-of-phase signals between water and methylene in the MGE sequence (Table 4). At 1.5 T, every in- and out-of-phase position was acquired. At 3 T, every third was collected due to the larger chemical shift between fat and water at the higher field strength. At both field strengths, a monopolar acquisition was used. Three T_1-weightings were used at every scanner in order to test three options of reducing T_1-bias. A flip angle of 15° and a TR of 1200 ms were used to test the small flip angle method. Using these parameters, the longitudinal magnetization was approximately 98 % of M_0 for water and 100 % for fat. The dual flip angle method was tested through the use of the flip angles 20° and 60°, both with a TR of 800 ms. The field of view (FOV) was larger at 1.5 T because of a lower gradient strength compared to the 3 T scanner.

SNR in the first echo ranged from approximately 140-660 in the tube with pure Intralipid depending on field strength and flip angle. The corresponding values for the vial containing only water varied from 230-550.

Table 4. Imaging and spectroscopy parameters used during the Intralipid phantoms experiment.

	Monopolar MGE, 1.5 T	*Monopolar MGE, 3 T*	*PRESS, 1.5 T*	*PRESS, 3 T*
Echo shift (°)	180	540	-	-
Number of echoes	10	10	-	-
TE (ms)	2.21, 4.42, 6.63, 8.85, 11.06, 13.27, 15.48, 17.69, 19.90, 22.12	2.29, 5.71, 9.14, 12.57 16.00, 19.43, 22.85, 26.28 29.71, 33.14	30	30
TR (ms)	1200, 800	1200, 800	7000	7000
Flip angle (°)	15, 20, 60	15, 20, 60	-	-
Slice thickness (mm)	5	5	-	-
Matrix	256x256	256x256	-	-
FOV (mm^2)	193x280	190x190	-	-
Bandwidth (Hz/pixel)	700	500	1200	1200

	Monopolar MGE, 1.5 T	*Monopolar MGE, 3 T*	*PRESS, 1.5 T*	*PRESS, 3 T*
NEX	4	4	32, 64, 128[1]	32, 64, 128[1]
Voxel size (mm^2)	-	-	10x10x22	7x7x18

3.2.1. T_1- and T_2-measurements

T_1 and T_2 were determined by turbo spin echo inversion recovery (IR) and multi echo spin echo (SE) sequences, respectively. Relaxation times of water were taken to be the relaxation times of the most diluted doped Intralipid phantom and the relaxation times of fat were measured in a rapeseed oil sample. In the IR sequence, the time of inversion was varied and in the SE sequence the echo times, keeping the remaining parameters fixed. The parameters used are summarized in Table 5. The same parameters were used in both 3 T and 1.5 T Siemens scanners.

T_1, T_2, M_0 and k were solved iteratively through curve fitting of the acquired data to IR (Eq.15) and SE (Eq.16) signal equations, respectively [12]. The fitting was performed in *Microsoft Office Excel 2003*. M_0 represent the signal unaffected by T_1- and T_2-relaxation, *TI* the time from inversion and k is a factor that depends on the quality of the inversion pulse.

$$S_{IR} = M_0 \cdot \left(1 - k \cdot e^{-\frac{TI}{T_1}} + e^{-\frac{TR}{T_1}} \right) \quad \text{(Eq.15)}$$

$$S_{SE} = M_0 \cdot e^{-\frac{TE}{T_2}} \quad \text{(Eq.16)}$$

In order to separate the T_2-values of the methylene and the remaining fat signal components in rapeseed oil, data was fitted to a sum of four exponential expressions corresponding to contributions of four different fat protons. The largest M_0 was assigned to belong to methylene and the average T_2 of fat was calculated as a weighted average of the four.

Table 5. Parameters used for T_1- and T_2-relaxation measurements.

	Multi contrast spin echo	*Fast spin echo inversion recovery*
TR (ms)	3000	3500
TE (ms)	15, 30, 45, 60, …, 465, 480	10
TI (ms)	-	50, 100, 200, 400, 800, 1600, 3200
Matrix	128x128	256x256
Echo train length	32	9
Slice thickness (mm)	5	5

3.3. Animal experiments

Twelve rats were fed daily with a steatosis-inducing drug during one month after which they were imaged in a 4.7 T Bruker scanner, using a four-element coil array. (Because of problems with compatibility of the pulse sequences and the coil array, only two of the coil elements could be used.) The animals were put under anaesthetics and were placed in the prone position, feet first in the scanner. They were monitored by electrocardiography (ECG), breathing rate and rectal temperature.

First, fast gradient echo scans of short-axis slices covering the heart from the apex to the base were repeated during the entire ECG cycle in order to create a cine-movie. From these

[1] The number of signal averages was governed by the expected fat fraction, where a higher number was used in phantoms with lower fat contents to improve SNR.

scans, stroke volume and ejection fraction were determined as measures of cardiac function. The analysis and results of these measurements are beyond the scope of this work. After this, an ECG-triggered and breathing-gated spectroscopy measurement localized in the cardiac septum using a PRESS-sequence with the parameters summarized in Table 6. These results were analyzed as described in Section 3.4.2.

Finally, a MGE sequence was used to scan three short-axis slices through the ventricles. Data acquisition was triggered to ECG and gated to breathing. The echo times were calculated to yield every third in- and out-of-phase position between water and methylene of rapeseed oil (-3.3 ppm). Both monopolar and bipolar acquisitions was used. Other parameters used are presented in Table 6. SNR (according to Eq.13) in the first echo of this series ranged from 60-110. In order to maximize the thickness of the cardiac muscle and thereby the number of pixels to be evaluated, data acquisition was performed during systole. The delay from the QRS-complex of the ECG signal to systole was determined from the cine-movie. The resulting images were analyzed according to Section 3.4.1. The fat model was shifted to make the methylene/water shift of the model match the shift measured in spectroscopy.

Regions of interest were drawn anteriorly in the myocardium in each slice of each rat.

Table 6. Parameters used for imaging with monopolar data collection

	Monopolar MGE	*PRESS*
Number of echoes	8, 11[1]	-
TE (ms)	3.0, 6.8, 10.6, 14.3, 18.1, 21.9, 25.6, 29.4…	7
TR (ms)	400 – 500 governed by heart rate	3000
Flip angle	50°	-
Matrix	128x128	-
NEX	10	96
Voxel size (mm)	-	3x2x2

3.4. Reconstruction and data analysis

3.4.1. Imaging

The reconstruction algorithm used in this work was implemented in *Matlab* (version R2008a). From the Bruker scanner, the raw signal data was extracted and reconstructed to complex images. From the Siemens scanners, magnitude and phase images were saved and from these, magnitude and complex data were obtained.

In order to shorten the reconstruction time, the data was first limited by excluding pixels only containing noise. For the remaining pixels, the complex data was off-resonance corrected as described in Section 2.2.2. After this a pixel-by-pixel iteration solving for the complex field map (or T_2* in case of a magnitude reconstruction) was performed using the method presented in Section 2.2.2. The iterations continued until the calculated correction was below 0.01 Hz or until a maximum number of 10 iterations were reached. These steps always included all collected echoes.

Fat-fat interactions were dealt with by using a pre calibrated Intralipid model with nine fat peaks (Table 2). Based on the calculated complex field map or T_2*-map, the fat and water signal contributions were estimated using Eq.4. In this estimation of fat and water signals, the number of echoes used could be varied. For *in vitro* data, only the first three echoes were used

[1] The number of echoes depended on T_2* where only as many echoes that was considered useful was acquired.

in this step. For *in vivo* data, reconstructions using all and only the first three echoes were performed.

Finally, the signal values were corrected for T_1-relaxation and ρ differences between water and fat using Eq.9. Alternatively, the fat and water estimates were reconstructed also for data collected with a second flip angle, and T_1-corrected data was estimated as described by Eq.10 and Eq.11. No T_1-correction was considered necessary for the reconstruction of small flip angle data. T_2-relaxation was corrected for by an inclusion of this parameter in the matrix A (see Section 2.2.3) when evaluating phantom data, while it was not accounted for in the evaluation of animal data. The volume fat fraction was calculated based on Eq.1.

Regions of interest were drawn, and within these the mean values and standard deviations of the estimated volume fat fractions were calculated. Only the median 50 % of the estimated values within the ROI were used in order to avoid extreme values in pixels where the reconstruction did not converge.

3.4.2. Spectroscopy

The acquired FID was zero-filled and apodized before Fourier transform. After this, baseline and phase corrections were made and finally a curve fitting of the water and methylene peak was performed. The chemical shift was determined from the positions of the water and methylene peaks. In order to determine the fat fraction (Eq.1), the integrals of the respective peaks were corrected for T_1- and T_2-relaxation, using Eq.14, as well as proton density differences. In order to also take non-methylene protons into account, the methylene integral was increased by a factor 1/0.6148, 0.6148 is the relative integral of the methylene peak in an Intralipid spectrum (Table 2).

4. Results

4.1. Simulations

Simulating an SNR of 70 and a ROI containing 100 pixels, the standard error of the mean (SEM) of the average fat fraction within the ROI was approximately determined to 0.02 %, using the Ernst angle of water. This indicates that the smallest detectable fat fraction approximately was 0.04 % when limited only by noise propagation. If the small flip angle approach was used, this limit was raised to about 0.08 %. Using only the first three echoes in the reconstruction barely doubled the smallest detectable fat fraction.

Figure 7 shows the results from a simulated echo collection at 1.5 T and 3 T, with water and fat being exactly in- and out-of-phase and slightly off these positions. While a complex reconstruction was entirely insensitive to the echo shift, the magnitude reconstruction underestimated the fat fractions even with the methylene peak being exactly in- and out-of-phase. This tendency was larger at 3 T where the echo shift was 540° instead of 180° due to the higher frequencies.

The results from simulations of the reconstructions using inaccurately modelled fat/water shift for magnitude and complex data from 1.5 T and 3 T scanners are shown in Figure 8. Again, 1.5 T proved to be less sensitive to errors and uncertainties in the method. A use of fewer echoes in the estimation of fat and water reduced the underestimation caused by inaccuracies in the fat model position relative to the water peak position.

Simulations performed to optimize the imaging parameters showed that with a fixed maximum scan time, the choice of repetition time was not critical for noise performance in the estimated fat fraction. The optimal choice of flip angle is illustrated in Figure 9, where the flip angle corresponding to the maximum SNR in the estimated signal and volume fat fractions are compared to the Ernst angles of fat and water. Interestingly, the Ernst angle of water is seen to be an optimal choice to improve SNR in the estimated signal fat fraction at low fat fractions whereas the SNR of the estimated volume fat fraction is maximized at the Ernst angle of fat at any simulated fat fraction.

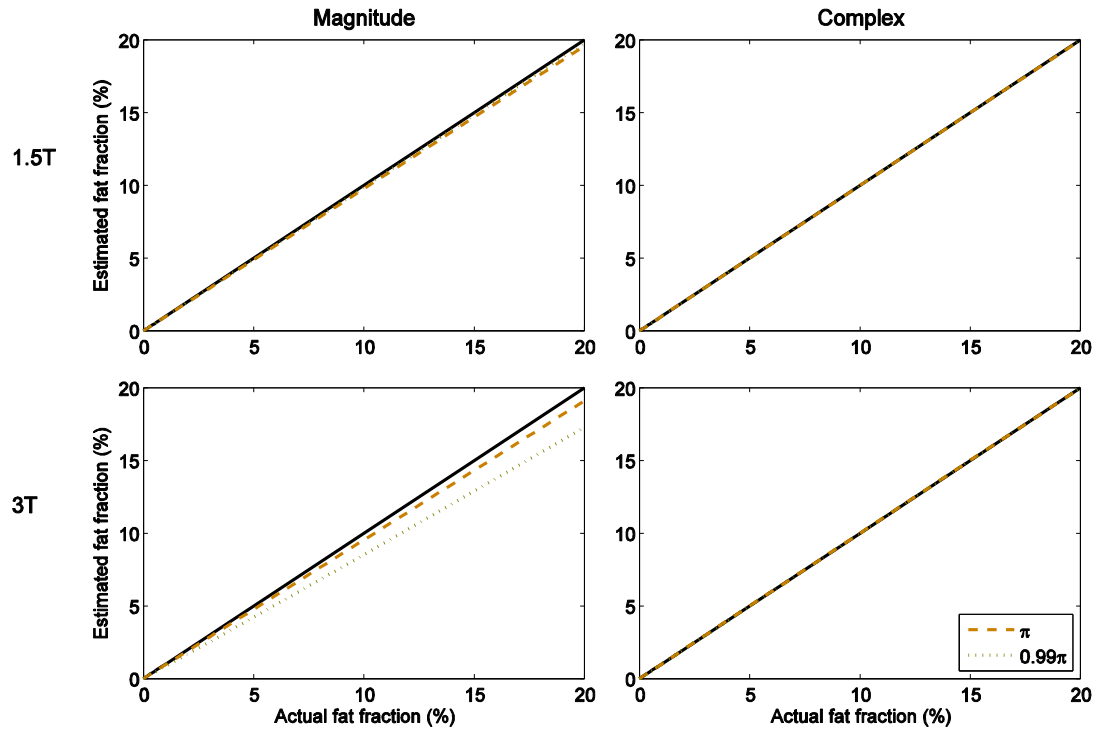

Figure 7. Simulated fat fractions at 1.5 T and 3 T, using magnitude and complex data. The data has been simulated to be collected when the methylene peak is exactly in- and out-of-phase (brown dashed line) from water, and 99% of in- and out-of-phase (green dotted line). The line of identity is shown in black.

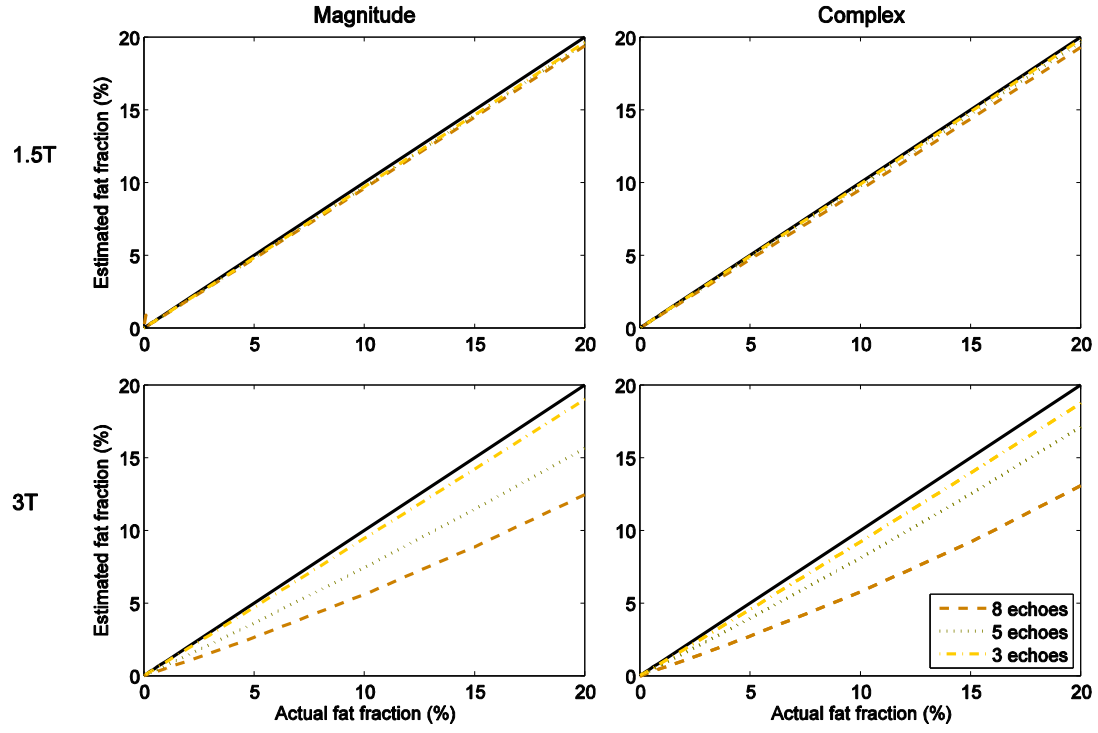

Figure 8. Magnitude and complex reconstruction using a slightly shifted fat model relative to the true fat spectrum at 1.5 T and 3 T. In the reconstructions, all eight echoes were used in the field and T_2*-iterations, but only eight (brown dashed line), five (green dotted line) or three echoes (yellow dash-dotted line) in the estimation of fat and water. The line of identity is shown in black.

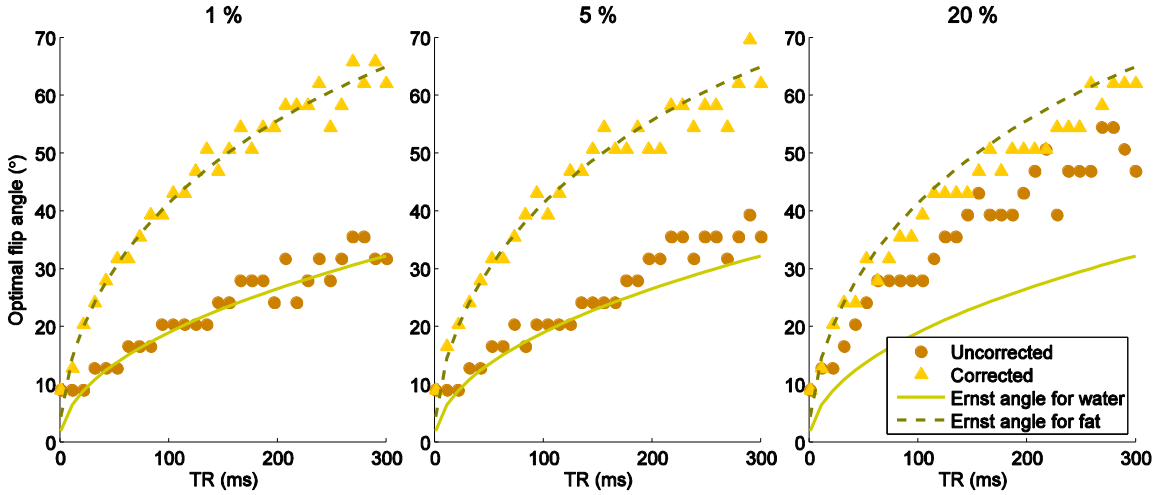

Figure 9. Optimal flip angles for maximized SNR in T_1 and ρ uncorrected (brown circles) and corrected (yellow triangles) estimated fat fractions using simulated fat fractions of 1 %, 5 % and 20 %. The Ernst angles of fat and water are shown as green dashed and solid lines respectively.

4.2. Phantom measurements

The results from the phantom study are summarized in Figures 10-12 and Table 7. Table 7 summarizes the results from an analysis of the regression between real and estimated volume fat fractions from spectroscopy and the small and dual angle imaging methods using magnitude and complex data at the two field strengths. All methods except spectroscopy at 1.5 T had slopes that were significantly different from one (ANOCOVA, $p<0.05$), but no method had an intercept that was significantly different from zero.

For both small and dual angle methods (Figures 11-12), the estimated fat fractions were slightly underestimated. This underestimation was significantly more pronounced for all methods at the higher field strength. The slightly increased underestimation using magnitude compared to complex data was not significant for any method. The standard deviation of the estimated volume fat fraction was larger using the small angle approach compared to using the dual angle method, but the methods were significantly different only when using magnitude data at 3 T.

The imaging methods accurately quantified volume fat contents and the accuracy was similar to that of spectroscopy. However, the slopes for all imaging methods but the dual angle method using complex data at 3 T were significantly different from the spectroscopy results. The imaging methods were also accurate at very low fat fractions with a lowest quantified volume fat fraction of approximately 0.2 %.

Using a T_1-corrected method (Figure 10), the estimated fat fractions were increasingly underestimated with a higher flip angle.

Figure 13 shows an example data from first echo image, the estimated water and fat images and the calculated volume fat fraction image (%).

Table 7. Results from an analysis of the regression between actual and estimated volume fat fraction for imaging and spectroscopy at 1.5 T and 3 T. Slopes are indicated by *a* and intercepts as *b*. Small and dual flip angle approaches were compared as well as using magnitude or complex data in the reconstruction. 95 % confidence intervals are given. Asterisks indicate a statistically significant difference from a slope of 1 and an intercept of 0.

		1.5 T		***3 T***	
		Small flip angle	*Dual flip angle*	*Small flip angle*	*Dual flip angle*
Imaging (%)	*Magnitude*	*a*: 0.895 ± 0.012* *b*: -0.18 ± 0.17	*a*: 0.935 ± 0.022* *b*: -0.10 ± 0.32	*a*: 0.8027 ± 0.0086* *b*: -0.21 ± 0.12	*a*: 0.851 ± 0.011* *b*: -0.16 ± 0.15
	Complex	*a*: 0.913 ± 0.012* *b*: -0.15 ± 0.17	*a*: 0.952 ± 0.023* *b*: -0.05 ± 0.33	*a*: 0.840 ± 0.010* *b*: -0.23 ± 0.14	*a*: 0.882 ± 0.012* *b*: -0.15 ± 0.18
Spectroscopy (%)		*a*: 1.029 ± 0.010 *b*: 0.11 ± 0.15		*a*: 0.898 ± 0.011* *b*: -0.21 ± 0.16	

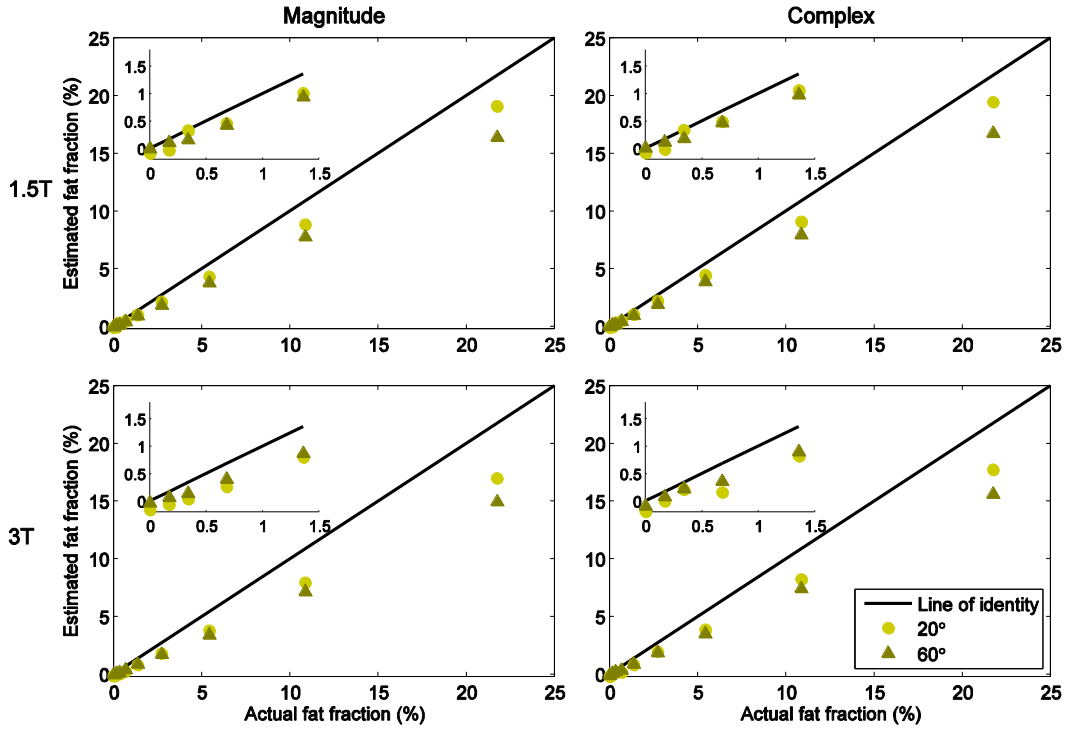

Figure 10. Comparison of results using the flip angles 20° (light green circles) and 60° (dark green triangles) at 1.5 T and 3 T, using magnitude and complex data in the T_1-corrected reconstruction. The line of identity is shown in black and the insets show enlargements of the diagrams at small FFs.

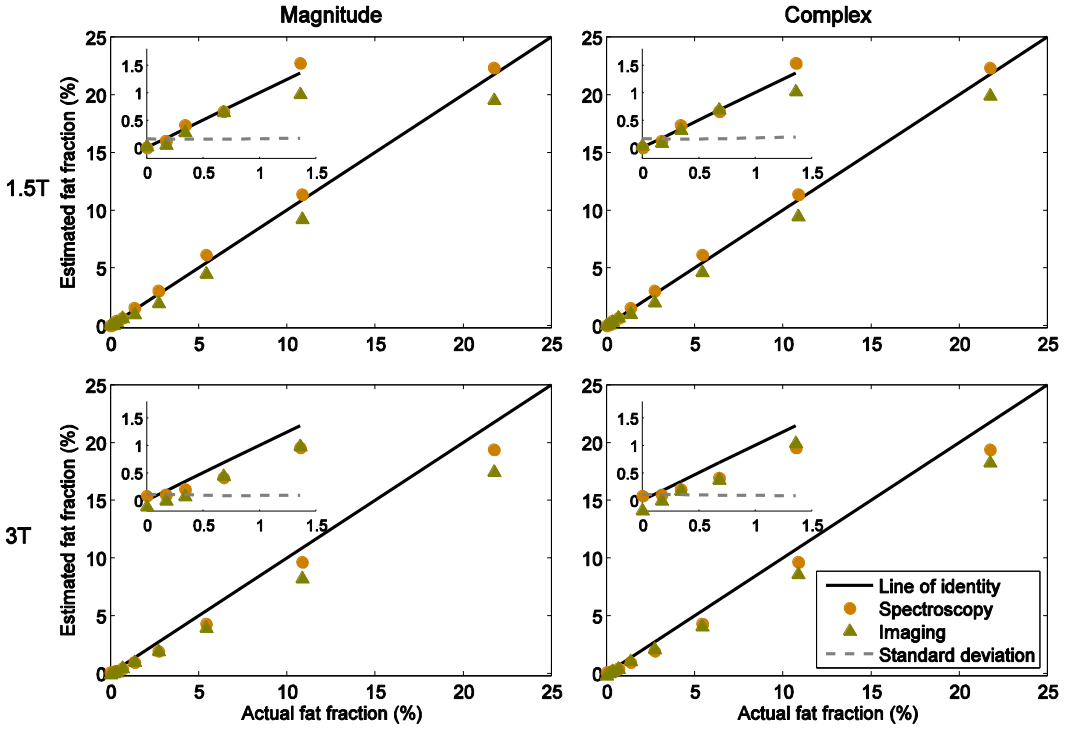

Figure 11. Comparison of results from imaging (green triangles) and spectroscopy (brown circles) at 1.5 T and 3 T, using magnitude and complex data using a small angle reconstruction. The line of identity is shown in black and the imaging standard deviation in dashed grey. The insets show enlargements of the diagrams at small FFs.

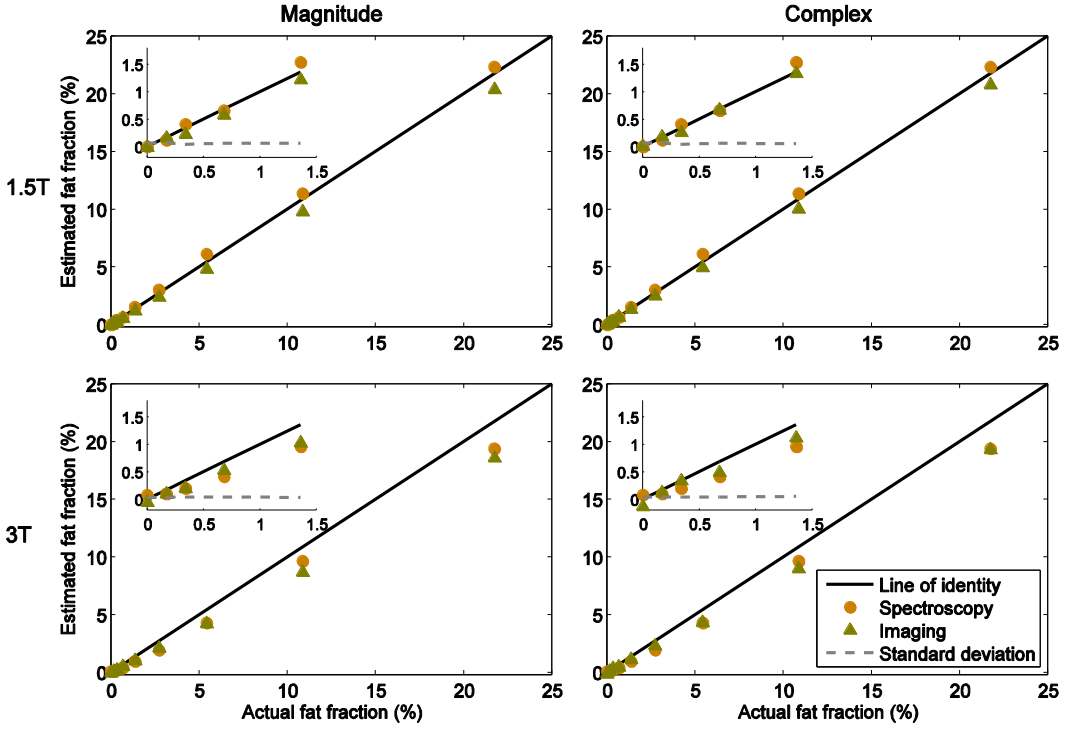

Figure 12. Comparison of results from imaging (green triangles) and spectroscopy (brown circles) at 1.5 T and 3 T, using magnitude and complex data using a dual angle reconstruction. The line of identity is shown in black and the imaging standard deviation in dashed grey. The insets show enlargements of the diagrams at small FFs.

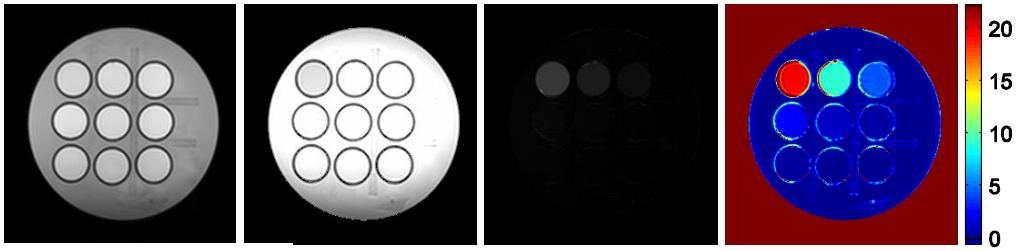

Figure 13. Example of results from the phantom study at 3 T. Shown in the figure are (from left): The first collected echo, the estimated water image, the estimated fat image and the estimated fat fraction image (%).

4.2.1. T_1 and T_2-measurements

The relaxation parameters of water in Intralipid and fat in rapeseed oil at 1.5 T and 3 T are summarized in Table 8. These values were used in the reconstruction of phantom data, as described in Section 3.1.

Table 8. Measured relaxation parameters at 1.5 T and 3 T in the water component of the most diluted doped Intralipid phantom and in rapeseed oil.

1.5 T			***3 T***		
	T_1 (ms)	*T_2 (ms)*		*T_1 (ms)*	*T_2 (ms)*
Water (Intralipid)	1070	880	*Water (Intralipid)*	1140	890
Fat (Average)	220	100	*Fat (Average)*	290	120
Methylene	-	50	*Methylene*	-	50

4.3. Animal experiments

Results from the quantitative histological analysis were not complete at the time of writing and therefore results presented here are from the qualitative evaluation. Results from spectroscopy and histology are summarized in Table 9. No fat peak could be detected in animal 10 and no spectroscopy measurement was performed in animal 4. An example of the results from animal 6 is shown in Figure 14 where the first acquired echo is seen together with reconstructed water, fat and fat fraction images. Far to the left, the T_2*- and off-resonance-map are presented.

Average fat fractions in three slices per animal using all or only the first three echoes in the reconstruction are shown in Figure 15. As can be seen, the results are very much affected by a change in reconstruction method and it is impossible to determine which method yields the most trustworthy result or which animal has the most elevated fat content. In Figure 16 results from the imaging method is compared to results from spectroscopy. Unfortunately, the comparison indicates no correlation between spectroscopy and any of the imaging methods. However, histology results do correlate significantly with spectroscopy results, but with neither of the imaging methods.

As the reconstruction did not converge in the case of bipolarly collected data, this data set could not be evaluated and no results are presented here.

Table 9. Results from spectroscopy measurements and preliminary histology evaluation

Animal	*Fat fraction (%)*	*Water/Methylene shift (ppm)*	*Perceived spectrum quality*	*Degree of steatosis according to histology*

Animal	*Fat fraction (%)*	*Water/Methylene shift (ppm)*	*Perceived spectrum quality*	*Degree of steatosis according to histology*
3	1.89	– 3.40	Very good[1]	Minimal
4	-	-	Spectroscopy not performed	Minimal
5	0.68	– 3.38	Good	Mild
6	0.26	– 3.43	Good	None
7	0.83	– 3.35	Good	Mild
8	0.74	– 3.42	Good	Mild
9	0.45	– 3.38	Good	Mild
10	-	-	Very poor	Mild
11	1.23	– 3.36	Very poor	Mild
12	0.37	– 3.41	Very poor	Mild
13	0.19	– 3.43	Poor	Minimal
14	0.39	– 3.32	Very poor	Minimal

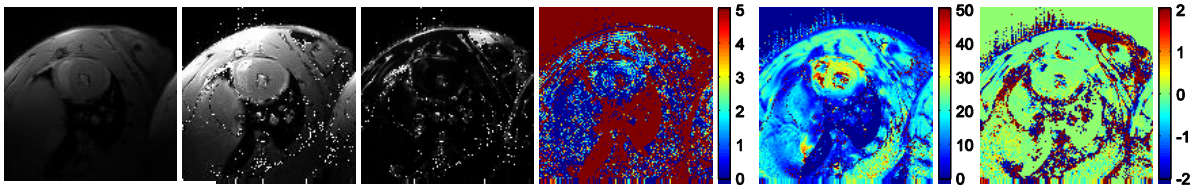

Figure 14. From left: The first collected echo in animal nr 6, estimated water image, estimated fat image, estimated fat fraction image (%), estimated T_2*-map (ms) and field map after off-resonance correction (Hz).

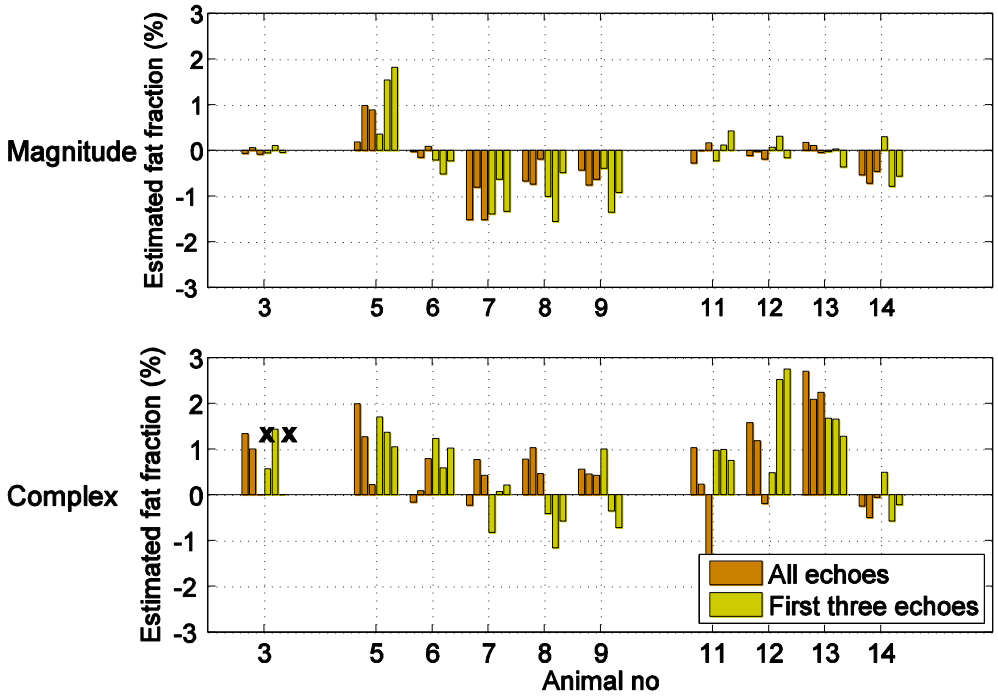

Figure 15. Estimated fat fraction in ROIs drawn in three slices per animal. Reconstructions were made using both magnitude and complex data and as well as using all (brown bars) and only the first three echoes (green bars) in the estimation of the fat fractions. x indicates that the fat fractions could not be evaluated due to artefacts.

[1] The quality of the fit was very good, but the voxel was placed such that the risk of contamination was increased

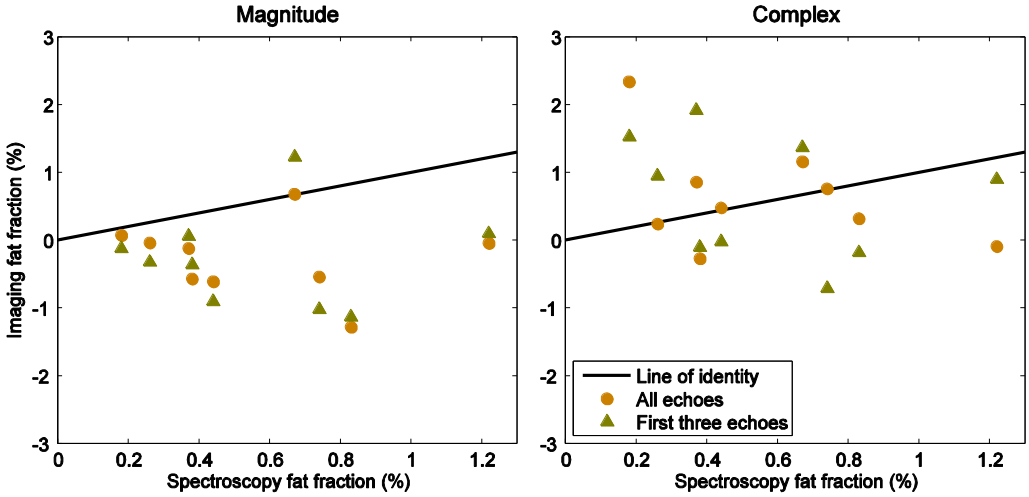

Figure 16. Comparison between the spectroscopy and imaging method of fat quantification using magnitude and complex data and using all (brown circles) or only the first three echoes (green triangles) in the reconstruction. The black line show the line of identity.

5. Discussion

The developed imaging method to quantify intra-myocellular fat content has been successfully tested *in vitro* in this work. Using a phantom study, the accuracy of the imaging method was shown to be similar to the quantification accuracy of spectroscopy and even very low fat fractions were successfully detected and quantified. However, *in vivo* the method was not able to accurately quantify the low fat fractions estimated through spectroscopy and histology.

The novelties of this work is the use of as many as 8-11 echoes in the estimation of the field inhomogeneity maps, but only three echoes in the estimation of the fat fraction. Also, the inclusion of T_2 of water and fat in the matrix A is introduced in this thesis and the inclusion of as many as nine fat peaks in the fat model is more thorough than what has been done in other works [10,20].

The advantage of using an imaging based method compared to MRS is the possible detection of a heterogeneous distribution of the accumulated fat. Another important advantage is that while the voxel shape in spectroscopy is limited to a cube, any shape can be given to the region of interest that is to be evaluated using the imaging method. Also, in spectroscopy the voxel placement is difficult, especially as the water and fat voxel will be shifted from each other due to a chemical shift artefact. These problems will be particularly limiting in the heart where macroscopic movements make the positioning of the voxel especially challenging.

Spatial information can also be obtained using MRSI. However, the long acquisition time connected with the phase encoding technique in two or three dimensions make the practically achievable resolution low. As for detection of heterogeneous fat accumulation patterns and detail, MRSI therefore cannot compete with the imaging technique developed here.

A possible disadvantage of using imaging as opposed to both spectroscopy methods is the inability of the imaging method to distinguish between IMCL and EMCL. However, in the heart, no EMCL is expected to be present. In addition, the resolution of measured spectrums may not be high enough to make this distinction even when using spectroscopy in the case of measurements in the heart.

Using magnitude and complex data in the reconstruction both have their respective advantages and disadvantages. Using a magnitude reconstruction, off-resonance effects are entirely avoided and possible disturbances from phase errors due to flow effects should be reduced. Even if the off-resonance effects are corrected for by the use of two methods while using complex data, animal data still show artefacts. These artefacts could be due to unsuccessful unwrapping during the off-resonance correction and other techniques will be investigated further. The off-resonance correction, which is based on the assumption that the fat fractions are very low, will possibly cause higher fat fractions to be inaccurately quantified. This will also need to be studied further in the future.

Unfortunately, simulations show that the choice of echo times is much more critical in case of magnitude data. Using complex data, this is not a problem, since any echo times can be used (except for an echo shift of 360°). The uncertainty in the choice of echo times can be minimized by initiating measurements with a PRESS sequence from which the chemical shift between water and methylene can be calculated. Using this shift and the known resonance frequency of water, the echo times can be chosen to yield in- and out-of-phase signals from water and methylene. Due to fat-fat interactions also this is a simplification. The total fat magnetization vector, containing signal from all fat peaks, will not be exactly in- and out-of-phase even if the methylene signal is. This causes the estimation of the fat fraction to always

be slightly underestimated when using magnitude data (see Figure 7). Uncertainties in the fat peak positions compared to the water peak position are such that perfect in- and out-of-phase signal collection is difficult to achieve. In addition, an equidistant distribution of echoes makes a perfect signal acquisition impossible.

The strength and speed of the gradients will govern the minimum possible echo shift. At higher field strengths, the resonance frequencies of water and fat are higher and the echoes need to be collected closer together in order to collect every in- and out-of-phase time point. This requires that the gradients are strong enough to handle the faster echo acquisition. At the 3 T and 4.7 T scanners used in this study the shift had to be chosen to 540° instead of 180°. This explains why the use of higher field strengths tends to be much more sensitive to accurate positioning of the fat model and the choice of echo times. It does not however explain why also the spectroscopy measurements underestimate the fat fraction at 3 T (Figure 11-12). At present, no explanation of this can be given.

Due to the rather small differences in frequencies between the fat peaks, earlier echoes will not be as affected by fat-fat interactions as the later echoes. Because of this, a slightly inaccurately positioned fat model will have an increased importance at later time points. Later echoes are, for the same reason, more deviant from the in- and out-of-phase position of water and fat. This means, that at higher field strengths the importance of accurately chosen echo times and fat model peak positions compared to the water peak position is much more crucial. In order to reduce this sensitivity it is possible to use fewer echoes in the estimation of fat and water. However, using fewer echoes also in the estimation of T_2* and complex field map lead to inaccurate correction of these effects. Fat-fat interactions will affect the signal over time in a way that yields an apparent increase of the T_2*-effect. In order to correctly separate the effects, more information of the signal needs to be used.

The use of all acquired echoes to estimate these field inhomogeneity maps in combination with the use of only three echoes to estimate the fat and water signals is considered one of the major contributing factors to the successful quantification shown here.

In order to be able to evaluate the bipolarly acquired data set, more work is needed. Bipolar acquisition strategies are known to cause phase errors due to misalignments in k-space between different echoes, but a further investigation of the problems encountered here are beyond the scope of this work [21].

Although the resonance frequencies of fat in Intralipid and IMCL should be similar due to the similarities in bulk susceptibility effects, it is not certain that the amplitudes are comparable. The amplitudes of the fat structure will instead be dependent on the type of fatty acids that make up the triacylglyceride molecule. By the use of Intralipid as a fat model, the fat stored in muscle cells are approximated to be similar to soybean oil. This needs further investigation.

There are three possible ways to deal with T_1-bias. The small flip angle method will not completely eliminate the effect but, theoretically, the dual flip angle method will. Using the small angle approach will also reduce the SNR. A third option is to use the signal expression for a gradient echo to correct for the bias by a known T_1-value. However, uncertainties in determining these T_1-values correctly, especially in mixtures of fat and water such as Intralipid, make this method hazardous. Inaccuracies in the effective flip angles compared to the nominal will also affect the results using this method, as the T_1-correction will be exaggerated when the effective flip angle is smaller than expected. This explains the increased underestimation of the fat fractions as the flip angle is increased in Figure 10. Inaccuracy in the effective flip angle is also a problem with the DESPOT-method that is the basis of the

dual flip angle method. According to Liu *et al.*, the uncertainties should however be eliminated through the calculation of the fat fraction [16]. One major disadvantage of this method is the double acquisition time.

In the future, it will be most interesting to measure T_2-values spectroscopically, using a range of echo times in several PRESS sequences. Here, a multi-exponential fitting was used which needs verification. However, T_2-values for fat and water will not be critical in the *in vivo* case, where field imperfections will render the difference in T_2-values negligible in comparison to the effects of T_2'.

In this work, quantification of low fat fractions has been demonstrated. The accuracy is highly dependent on a number of factors, such as a correct choice of echo shift as well as corrections for field inhomogeneities, T_2*-relaxation and fat-fat interactions. Estimation of the fat fraction in absolute terms as opposed to the signal fat fraction imposes the additional corrections for differences in relaxation times and proton density.

In order to increase the SNR of the estimated volume fat fraction, the Ernst angle of fat should be used. However, the SNR of the signal fat fraction was maximized by the use of the Ernst angle of water in both the phantom and animal experiments. This is thus an opportunity for further optimization of the imaging protocol.

Another possible strategy to improve the noise performance is the use of signals from both acquired flip angles in the calculation of the fat fraction. In this work, data from both flip angles have been used to estimate T_1-maps for water and fat, but only signal from the Ernst angle of water has been T_1-corrected and used to calculate the volume fat fraction. Instead, the sum of the signals using the two flip angles could be used.

The task of developing a method of quantification of intra-myocellular fat accumulation in the cardiac muscle of rats proved to have two major difficulties. The first of these is the expected low fat fractions of approximately 1 % even in animals with elevated fat content. In idealized circumstances, it is possible to quantify very low fat fractions, but *in vivo*, this is very difficult.

The second difficulty is the heart itself which is a problematic area to image and to evaluate through spectroscopy. The effects of macroscopic movement are reduced by triggering to ECG and gating to breathing, but these methods are not perfect.

Flow effects are expected to be eliminated through the use of magnitude data in the reconstruction which however increases the importance of carefully chosen echo times. Although spectroscopy could be performed prior to the multi-echo sequence, spectroscopy in the cardiac wall is difficult and the uncertainties are large, especially in case of low fat fractions. The effect of a suboptimal choice of echo times is further enhanced by the high field strength of the animal scanner.

Before a repeat of the study is performed, a careful phantom study similar to the one previously described should be conducted to verify the quality of the pulse sequence that is to be used at the Bruker scanner.

6. Conclusions

The developed imaging method does show potential to yield similar quantification accuracy as MRS, which is considered the golden standard of *in vivo* fat quantification. However, the method developed in this work also offers the opportunity to detect heterogeneous fat accumulation as well as being less sensitive to chemical shift artefact. Also, the method allows for evaluation of regions that may be shaped after the area of interest as opposed to MRS.

Quantification of intra-myocellular fat content has been shown to be possible and accurate for volume fat fractions as low as 0.2 % *in vitro* using the imaging method that was developed during this master thesis. Although this result has yet to be reproduced *in vivo*, the method does have potential to be applicable also in living tissue. This potential may be greater in organs were the fat content is higher and the movements less problematic than in the heart.

References

1. Gunstone FD, Harwood JL, Dijkstra AJ, editors. The Lipid Handbook. Boca Raton: CRC Press; 2007.
2. Boesch C, Slotboom J, Hoppeler H, Kreis R. *In Vivo* Determination of Intra-Myocellular Lipids in Human Muscle by means of Localized ^{1}H-MR-Spectroscopy. Magnetic Resonance in Medicine 1997;37:484-493.
3. Schrauwen-Hinderling VB, Hesselink MKC, Schrauwen P, Kooi ME. Intramyocellular Lipid Content in Human Skeletal Muscle. Obesity 2006;14(3):357-367.
4. Szczepaniak LS, Dobbins RL, Stein DT, McGarry JD. Bulk Magnetic Effects on the Assessment of Intra- and Extramyocellular Lipids in Vivo. Magnetic Resonance in Medicine 2002;47:607-610.
5. Lindsey JB, Marso SP. Steatosis and Diastolic Dysfunction: The Scinny on Myocardial Fat. Journal of the American College of Cardiology 2008;52(22):1800-1802.
6. MacGavock JM, Lingvay I, Zib I, Tillery T, Salas N, Unger R, Levine B, Raskin P, Victor RG, Szczepanik LS. Cardiac Steatosis in Diabetes Mellitus: A ^{1}H-Magnetic Resonance Spectroscopy Study. Circulation 2007;116:1170-1175.
7. Keevil S. Spatial localization in nuclear magnetic resonance spectroscopy. Physics in Medicine and Biology 2006;51:579-636.
8. Dixon TW. Simple Proton Spectroscopic Imaging. Radiology 1984;153:189-194.
9. Reeder SB, Wen Z, Yu H, Pineda AR, Gold GE, Markl M, Pelc NJ. Multicoil Dixon chemical species separation with an iterative least-squares estimation method. Magnetic Resonance in Medicine 2004;51(1):35-45.
10. Yu H, Shimakawa A, McKenzie C, Brodsky E, Brittain J, Reeder S. Multiecho water-fat separation and simultaneous R2* estimation with multifrequency fat spectrum modeling. Magnetic Resonance in Medicine 2008;60(5):1122-1134.
11. Rieke V, Butts Pauly K. MR Thermometry. Journal of Magnetic Resonance Imaging 2008;27:376-390.
12. Bernstein MA, King KF, Zhou XJ. Handbook of MRI Pulse Sequences. Amsterdam: Elsevier Academic Press; 2004.
13. Bydder M, Yokoo T, Hamilton G, Middleton MS, Chavez AD, Schwimmer JB, Lavine JE, Sirlin CB. Relaxation effects in the quantification of fat using gradient echo imaging. Magnetic Resonance Imaging 2008;26:347-359.
14. Yu H, McKenzie CA, Shimakawa A, Vu AT, Brau ACS, Beatty PJ, Pineda AR, Brittain JH, Reeder SB. Multiecho reconstruction for simultaneous water-fat decomposition and T2* estimation. Journal of Magnetic Resonance Imaging 2007;26(4):1153-1161.
15. Fernández-Seara MA, Song HK, Wehrli FW. Trabecular bone volume fraction mapping by low-resolution MRI. Magnetic Resonance in Medicine 2001;46(1):103-113.
16. Liu C-Y, McKenzie CA, Yu H, Brittain JH, Reeder SB. Fat quantification with IDEAL gradient echo imaging: Correction of bias from T1 and noise. Magnetic Resonance in Medicine 2007;58(2):354-364.
17. Glover G. Multipoint Dixon Technique for Water and Fat Proton and Susceptibility Imaging. Journal of Magnetic Resonance Imaging 1991;1:521-530.
18. Gudbjartsson H, Patz S. The Rician Distribution of Noisy MRI Data. Magnetic Resonance in Medicine 1995;34(6):910-914.
19. Stark DD, Bradley WGJ. Magnetic Resonance Imaging. St. Louis: Mosby; 1999.
20. Yokoo T, Bydder M, Hamilton G, Middleton M, Gamst A, Wolfson T, Hassanein T, Patton H, Lavine J, Schwimmer J, Sirlin C. Nonalcoholic Fatty Liver Disease: Diagnostic and Fat-Grading Accuracy of Low-Flip-Angle Multiecho Gradient-Recalled-Echo MR Imaging at 1.5 T. Radiology 2009;251(1):67-76.
21. Lu W, Yu H, Shimakawa A, Alley M, Reeder SB, Hargreaves BA. Water-Fat Separation with Bipolar Multiecho Sequences. Magnetic Resonance in Medicine 2008;60:198-209.

LUNDS UNIVERSITET